Projectile dependence of radioactive spallation products induced in copper by high-energy heavy ions

H. Yashima,[1] Y. Uwamino,[2] H. Sugita,[1] T. Nakamura,[1] S. Ito,[2] and A. Fukumura[3]
[1]*Department of Quantum Science and Energy Engineering, Tohoku University, Aoba, Aramaki, Sendai-shi 980-8579, Japan*
[2]*The Institute of Physical and Chemical Research, 2-1, Hirosawa, Wako, Saitama 351-0198, Japan*
[3]*National Institute of Radiological Sciences, 4-9-1, Anagawa, Inage-ku, Chiba 263-8555, Japan*
(Received 28 January 2002; published 9 October 2002)

Irradiation experiments were performed at the HIMAC (heavy-ion medical accelerator in Chiba) facility, National Institute of Radiological Sciences. The radioactive spallation products in a thick Cu target were obtained for 230 and 100 MeV/nucleon Ne, C, He, and *p* ions. The gamma-ray spectra from irradiated Cu pieces inserted into the composite Cu target were measured with a high-purity Ge detector. From the gamma-ray spectra, we obtained the variation of radioactive yields with depth in the Cu target and the mass-yield distribution of nuclides produced on the surface. The results show that the cross sections strongly depend on the projectile mass and, consequently, on the mass number difference between Cu and the produced nuclides. The most important feature of the present data is the extraction of the energy dependence of the cross sections. The measured cross sections were fitted to a modified form of Rudstam's semiempirical formula in order to evaluate the cross sections of unmeasured nuclides. These estimated cross sections were added to the experimental yields for each mass number and the total mass yield and isobaric charge distributions, and the slope of the mass-yield distribution were obtained.

DOI: 10.1103/PhysRevC.66.044607 PACS number(s): 25.70.Mn, 25.40.Sc, 29.25.Rm

I. INTRODUCTION

Recently high-energy and high-intensity heavy-ion accelerators are increasingly being used in nuclear physics, condensed matter physics, material damage study, and for medical applications, especially cancer therapy. At the National Institute of Radiological Sciences in Japan, the heavy-ion medical accelerator in Chiba (HIMAC) has been used for heavy-ion cancer therapy, and a similar facility is now operational at the Gesellschaft für Schwerionenforschung (GSI) in Darmstadt, Germany. Construction of new heavy-ion accelerator facilities for therapy has been started or is planned for the near future. Several institutions worldwide have started radioactive isotope beam facilities for investigating exotic nuclei, stellar nucleosynthesis, and so forth, including the Institute of Physical and Chemical Research (RIKEN), Japan, which uses a combination of cyclotrons. New large scale facilities are planned.

The safety design consideration for heavy-ion accelerator facilities requires the reaction cross section data for high-energy heavy ions to estimate the radioactivities induced in the accelerator components and in the shielding materials. Several studies on proton reaction cross section data have been done and a systematic study was carried out by Michel *et al.* [1–3], however, only a few studies on reaction cross section data for heavy ions have been reported [4–9].

Therefore, we decided to measure activation yields by irradiating a Cu target with 230 and 100 MeV/nucleon Ne, C, He, and *p* ions, which is a main element of accelerator components. Our aim was to investigate the projectile and energy dependencies of induced radioactivities of spallation products and to compare with existing data. The most important feature of the present data is the extraction of the energy dependence of the cross sections for proton and heavy-ion beams. We also fitted the measured cross sections to a modified form of Rudstam's semiempirical formula [10] by Porile, Cole, and Rudy [6] for evaluating the cross sections of unmeasured nuclides which are stable or have short (or very long) half-lives. These cross sections were added to the experimental yields for each mass number in order to obtain the experimental mass yield and isobaric charge distributions. We thus obtained the slope of the mass-yield distribution.

II. EXPERIMENTS

Irradiation experiments were performed at the HIMAC facility, National Institute of Radiological Sciences. A schematic view of the experimental setup is shown in Fig. 1. The natural Cu target consisted of a stack of two to seven 100 mm×100 mm×5 mm natural Cu plates, and the total thickness of the Cu target is a little thicker than the range of the projectile, that is, stopping length, as shown in Table I.

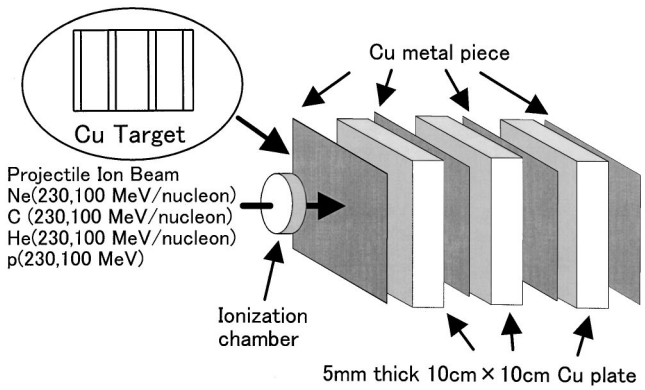

FIG. 1. Schematic view of the experimental geometry.

TABLE I. Conditions of irradiation experiments. ''short'' means for shorter irradiation time. ''long'' means for longer irradiation time.

Projectile and energy (MeV/nucleon)	Beam intensity (particles/sec)	Irradiation time (short/long) (min)	Target thickness (short/long) (g/cm^2)	Range (g/cm^2)
Ne[230]	5.03×10^8	61/364	9.89/14.62	9.79
C[230]	1.84×10^9	36/359	14.51/19.24	16.29
He[230]	9.15×10^9	21/304	55.60	48.86
p[230]	2.28×10^{10}	10/312	55.60	48.86
Ne[100]	7.40×10^8	31/366	5.06	2.37
C[100]	1.95×10^9	60/405	6.22	3.93
He[100]	1.05×10^{10}	48/360	14.79	11.76
p[100]	2.04×10^{10}	46/301	14.79	11.75

Only for 230 MeV/nucleon Ne and C irradiations, we used two different target thicknesses for shorter and longer irradiation time as shown in Table I. Up to eight Cu pieces, 0.1 mm thick, of chemical purity 99.9% were inserted between the 5 mm thick Cu plates. The Cu pieces put on the front surface were used for measurement of the reaction cross section and the mass-yield distribution of produced nuclides.

TABLE II. Estimated errors.

Component	Error (%)
Statistic error of total counts of gamma-ray peak area	1–40
Error of peak efficiency	0.5–7.2
Error of beam intensity	1–6
Total errors	2–40

The Cu pieces inserted between the Cu plates were used for measurement of the spatial distribution of the residual activities of produced nuclides in copper and for the energy dependence of the cross section. The irradiation experiments were carried out for four projectiles of fully stripped *p*, He, C, and Ne ions at energies per nucleon of 100 and 230 MeV, and the projectile dependence of the induced radioactivities of spallation products was investgated. The targets were irradiated both for a shorter irradiation time and a longer irradiation time, considering the half-lives of produced nuclei. An ionization chamber was placed in front of the target to monitor the beam current during irradiation, which was recorded by the digital current integrator, connected to a multichannel scaler with a dwell time of 10 s. The beam spot was less than 1 cm in diameter at the target position. The parameters of irradiation experiments are given in Table I.

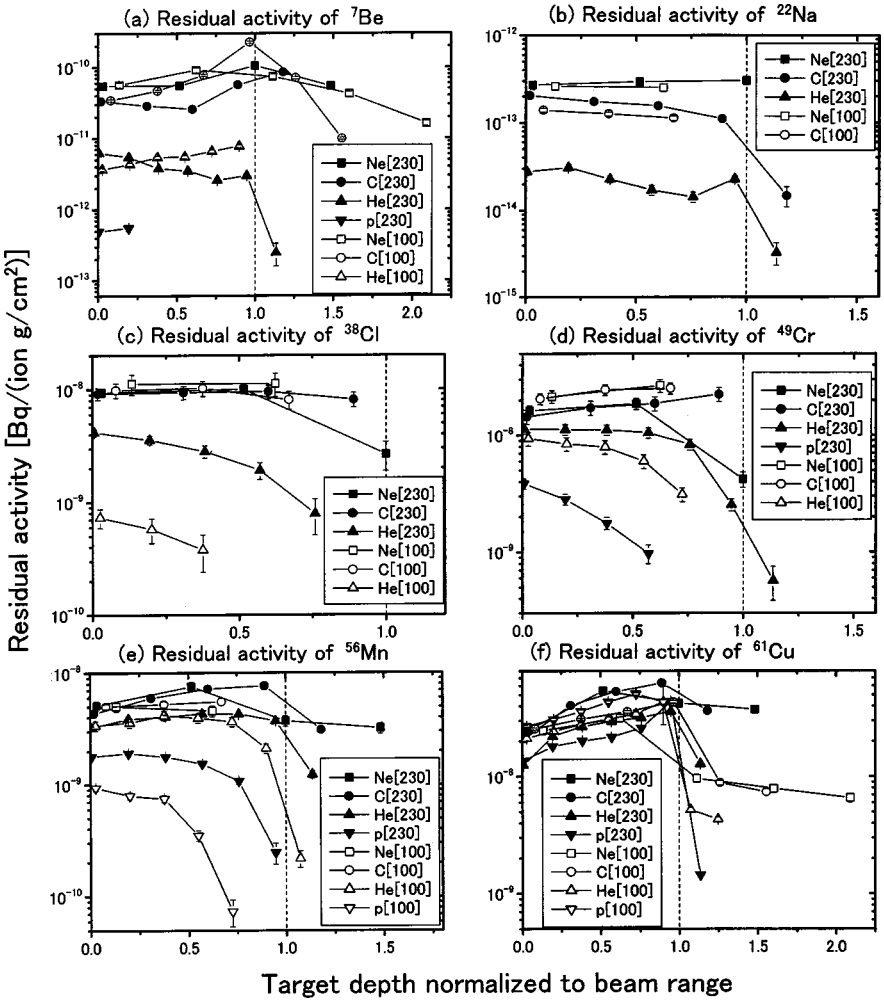

FIG. 2. Spatial distribution of residual activities within Cu target depth. For example, ''Ne[230]'' signifies 230 MeV/nucleon Ne irradiation.

The range of the projectile beam in copper was calculated by the SPAR [11] and ATIMA [12] codes, and the ranges given by both codes were in good agreement.

After irradiation, we measured the gamma-ray spectra from the Cu pieces with four high-purity germanium (HPGe) detectors (GC-1818, GC-2020, GX4019, and GC-3020, Canberra Industries) counted by 4096 multichannel analyzers. These Cu pieces were counted continuously at constant time intervals to identify the half-lives of the activities.

III. DATA ANALYSIS

The reaction rates of radionuclides produced in the Cu pieces, which were identified in the gamma-ray spectra, and the decay curves were determined after being corrected for the peak efficiency of the HPGe detector, the coincidence-summing effect, and for the beam current fluctuation during Cu piece irradiation. The peak efficiency of the HPGe detector was determined by using standard mixed gamma-ray sources and the electron-photon cascade EGS4 Monte Carlo code [13]. The coincidence-summing effect caused by coincident detection of two or more gamma rays in the gamma-ray spectrum was corrected by the SUMECC code [14]. This effect increases with decreasing Cu piece to detector distance.

The reaction rate per beam current R (C^{-1}), corrected for beam current fluctuation, is expressed by

$$R=\frac{\lambda C}{\varepsilon\gamma e^{-\lambda t_a}(1-e^{-\lambda t_m})\sum_{A=1}^{n}(Q_i e^{-\lambda(n-i)\Delta t})}, \qquad (1)$$

where λ is the decay constant (s^{-1}), C is the total counts of gamma-ray peak area, ε is the peak efficiency, γ is the branching ratio of gamma rays, Q is the beam current (C) for irradiation time interval $\Delta t(s)$, t_i is the irradiation time (s), $(t_i=n\Delta t)$, t_c is the cooling time (s), and t_m is the counting time (s).

From Eq. (1), we obtain the cross section σ (mb) in the Cu piece on the surface of the target and the residual activities A [Bq/(cm^2)] in the Cu pieces inserted between the Cu plates of the target by the following equations:

$$\sigma=\frac{RI}{N_d t}, \qquad (2)$$

$$A=\frac{\lambda RI}{t\rho}, \qquad (3)$$

where N is the number of atoms in the Cu piece (atom), I is the Coulomb per projectile ion, i.e., $Z\times 1.602\times 10^{-19}$ (C/projectile ion), Z is the atomic number of the projectile ion, N_d is the atomic density of the Cu piece (atom/cm^3), ρ is the density of the Cu piece (g/cm^3), and t is the thickness of the Cu piece (cm).

For nuclides where the fraction of the production by secondary particles is considered to be small, we could thus obtain the cross section in all Cu pieces inserted between the Cu plates by taking into account the projectile energy degradation in the target and the attenuation of projectile ions through the target due to multiple scattering. The energy and number of projectile ions through the target thickness d are calculated as follows:

TABLE III. Nuclides produced in Cu. *I* stands for independent, C^+ stands for cumulative positron, C^- stands for cumulative electron, *Y* stands for year, *D* stands for day, *H* stands for hour, and *M* stands for minute.

Residual nuclides	Type of yield	Gamma-ray energy (keV)	Branching ratio (%)	Half-life
^{7}Be	*I*	477.61	10.5	53.29*D*
^{22}Na	C^+	1274.53	99.9	2.6019*Y*
^{24}Na	C^-	1368.63	100	14.959*H*
^{27}Mg	C^-	843.76	71.8	9.458*M*
^{28}Mg	C^-	400.69	36.6	20.91*H*
^{29}Al	C^-	1273.3	90.6	6.56*M*
^{34m}Cl	C^+	146.36	40.5	32*M*
^{38}Cl	C^-	1642.71	31.9	37.24*M*
^{39}Cl	C^-	1267.18	53.6	55.6*M*
^{41}Ar	C^-	1293.59	99.1	109.34*M*
^{42}K	*I*	1524.7	18.1	12.36*H*
^{43}K	C^-	617.49	79.2	22.3*H*
^{43}Sc	C^+	372.76	22.5	3.891*H*
^{44}Sc	*I*	1157.03	99.9	3.927*H*
^{44m}Sc	*I*	271.13	86.7	58.6*H*
^{46}Sc	*I*	889.28	100	83.79*D*
^{47}Sc	*I*	159.38	68.3	3.3492*D*
^{48}Sc	*I*	1037.52	97.6	43.67*H*
^{48}V	C^+	983.52	100	15.9735*D*
^{48}Cr	C^+	308.24	100	21.56*H*
^{49}Cr	C^+	90.64	53.2	42.3*M*
^{51}Cr	C^+	320.08	10.1	27.702*D*
^{52}Mn	*I*	935.54	94.5	5.591*D*
^{52m}Mn	C^+	1434.06	98.3	21.1*M*
^{54}Mn	*I*	834.85	100	312.12*D*
^{56}Mn	C^-	1810.72	27.2	2.5785*H*
^{52}Fe	*I*	168.69	99.2	8.275*H*
^{53}Fe	C^+	377.9	42	8.51*M*
^{59}Fe	C^-	1291.6	43.2	44.503*D*
^{55}Co	C^+	931.1	75	17.53*H*
^{56}Co	C^+	1238.28	66.1	77.27*D*
^{57}Co	C^+	122.06	85.6	271.79*D*
^{58}Co	*I*	810.77	99.4	70.82*D*
^{60}Co	*I*	1173.24	100	5.2714*Y*
^{61}Co	C^-	67.42	84.7	1.65*H*
^{62m}Co	C^-	1163.5	68	13.91*M*
^{57}Ni	C^+	1377.63	81.7	35.6*H*
^{65}Ni	C^-	1481.84	23.6	2.5172*H*
^{60}Cu	C^+	1791.6	45.4	23.7*M*
^{61}Cu	C^+	282.96	12.2	3.333*H*
^{64}Cu	*I*	1345.77	0.47	12.7*H*
^{62}Zn	C^+	596.56	26	9.186*H*
^{63}Zn	C^+	669.62	8.2	38.47*M*
^{65}Zn	C^+	1115.55	50.6	244.26*D*

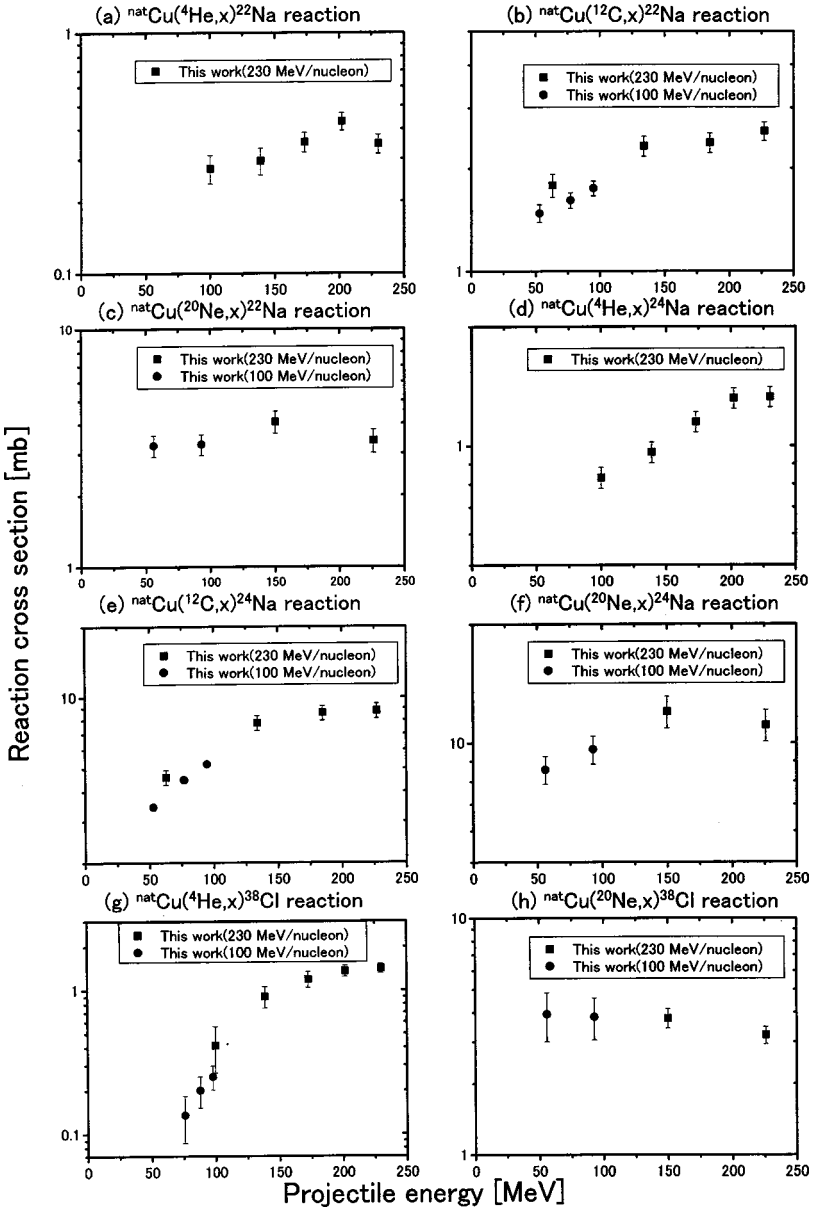

FIG. 3. Excitation function of nuclides produced in Cu. For example, "Ne[230]" signifies 230 MeV/nucleon Ne irradiation.

$$E = E_0 - \int_0^d \frac{dE}{dx} dx, \tag{4}$$

$$P = P_0 \int_0^d e^{-\sigma^{Tot}(E)N_d} dx, \tag{5}$$

where E is the energy of projectile ions through the target thickness d (MeV), E_0 is the incident energy of projectile ions (MeV), dE/dx is the stopping power calculated by SPAR code [11] (MeV/cm), P is the number of projectile ions through the target thickness d, P_0 is the initial number of projectile ions, and σ^{Tot} is the total reaction cross section calculated by Shen's formula [15] (cm^{-2}).

The estimated errors in the cross sections and in the residual activities are listed in Table II. Statistical errors of total counts in the gamma-ray peak area were 1–40 %. Errors of peak efficiency were calculated using the EGS4 code [13], and errors of beam intensity were determined from the beam current fluctuation during irradiation.

IV. EXPERIMENTAL RESULTS AND DISCUSSION

A. Domain of nuclides produced in Cu

We identified nuclides from ^{7}Be to ^{65}Zn in irradiated Cu pieces and the maximum number of 44 nuclides was obtained for 230 MeV/nucleon Ne irradiation. The list of nuclides produced in Cu is given in Table III and yields are denoted as independent (I), cumulative positron (C^+), and cumulative electron (C^-). The gamma-ray energies, the branching ratios, and the half-lives of produced nuclides are taken from Ref. [16] and half-lives vary between 7 min to 5 yr.

Once the nuclide is identified by gamma-ray energy and half-life, we obtain the cross section (mb) for one projectile ion in the surface of the Cu target and the residual activity

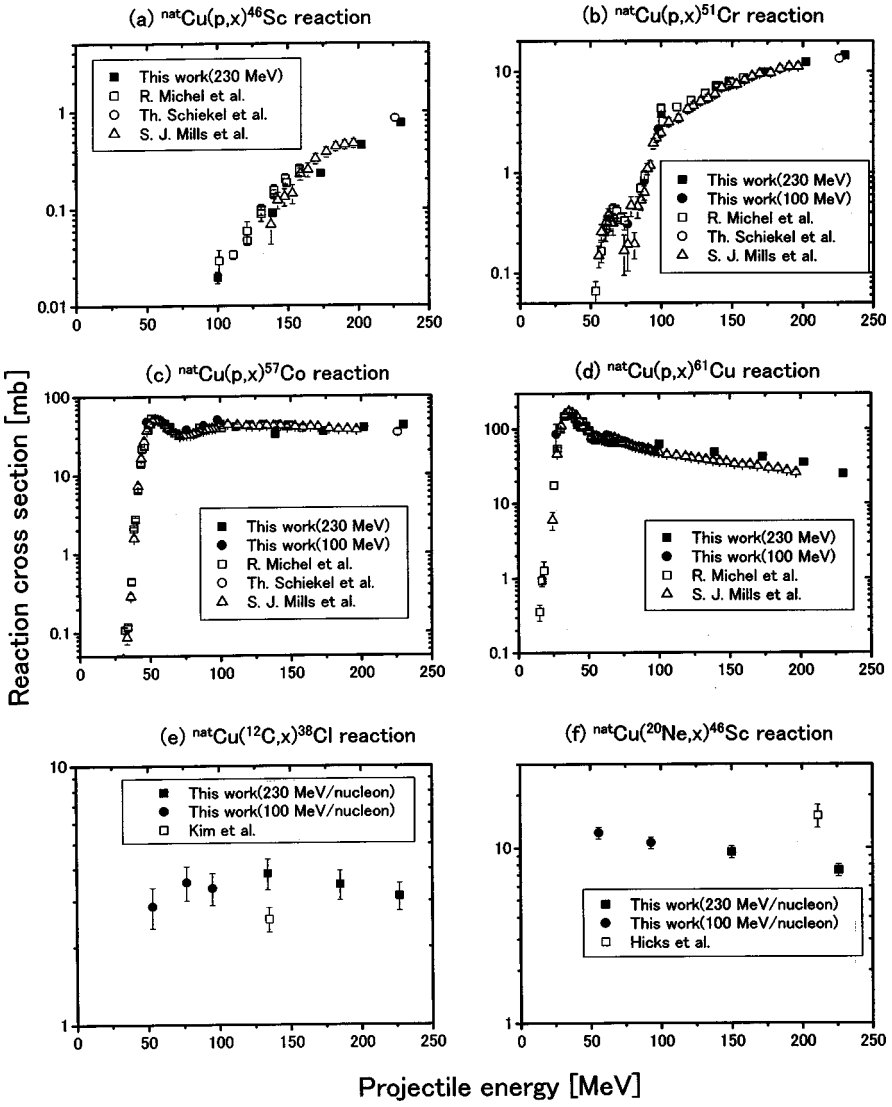

FIG. 4. Excitation function of nuclides produced in Cu. For example, "Ne[230]" signifies 230 MeV/nucleon Ne irradiation.

[Bq/(g/cm^2)] in Cu pieces inserted between the Cu plates. However, residual nuclides are produced not only by the primary projectile but also by secondary particles, and therefore the excitation function is deduced solely for nuclides where the fraction of production by secondary particles can be considered to be negligibly small. The excitation functions will be discussed later in Sec. IV C.

B. Spatial distribution of residual activities within Cu target depth

The spatial distribution of residual activities of ^{7}Be, ^{22}Na, ^{38}Cl, ^{49}Cr, ^{56}Mn, and ^{61}Cu is shown in Figs. 2(a)–2(f), respectively, where the target depth is expressed in units of the projectile range. The vertical dashed lines give the range of the projectile.

Figures 2(a)–2(f) can be understood and summarized as follows. When the mass number difference between Cu and the produced nuclide is large, nuclides are produced dominantly by the primary projectile. The reaction cross sections remain constant or slowly decrease with decrease in the target depth. When the mass number difference between Cu and the produced nuclide is small, the fraction of nuclides produced by reactions with secondary particles is large. With increasing mass number and projectile energy, the reaction cross section increases inside the Cu target as compared to the surface.

C. Excitation function of nuclides produced in Cu

Excitation functions were obtained for nuclides with mass numbers far from Cu, where the fractional production by secondary particles is considered to be small, taking into account the projectile energy degradation in the target by using the SPAR code [11] and the attenuation of projectile ion numbers through the target by using Shen's formula, as shown in Eqs. (4) and (5) [15]. The results are compared with existing experimental data [1–5,17]. In particular, for proton irradiation, the nuclides are essentially produced by energy-degraded primary protons. However, in the case of heavy-ion irradiation a fraction of nuclides is produced by secondary particles. In order to investigate the contribution from secondary-particle produced nuclides of mass numbers far from Cu target, we compared cross sections for 100

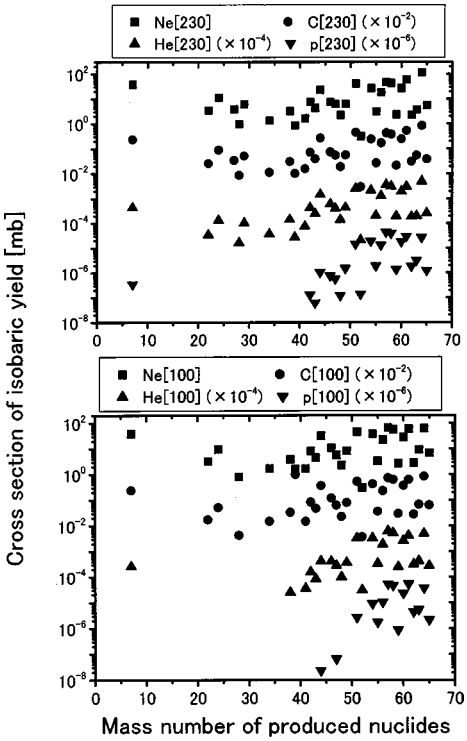

FIG. 5. Mass-yield (isobaric-yield) distribution of nuclides produced in Cu (upper, 230 MeV/nucleon; lower, 100 MeV/nucleon). For example, ''Ne[230]'' signifies 230 MeV/nucleon Ne irradiation.

MeV/nucleon beams with cross sections obtained for 100 MeV/nucleon degraded from 230 MeV/nucleon beams. These two data sets differ by less than 20% as shown in Figs. 3(b), 3(e), and 3(g), and consequently the contribution of spallation products induced by secondary particles must be considered but is relatively small.

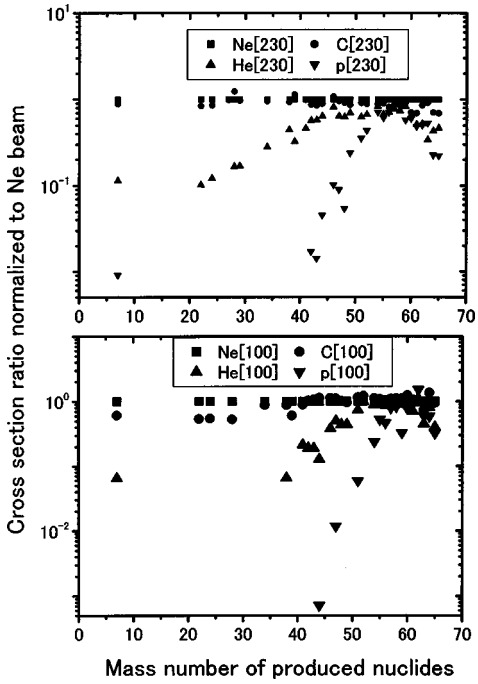

FIG. 7. Projectile dependence of nuclides produced in Cu (upper, 230 MeV/nucleon; lower, 100 MeV/nucleon). For example, ''Ne[230]'' signifies 230 MeV/nucleon Ne irradiation.

The excitation functions of $^{nat}Cu(p,X)^{46}Sc$, $^{nat}Cu(p,X)^{51}Cr$, $^{nat}Cu(p,X)^{57}Co$, $^{nat}Cu(p,X)^{61}Cu$, $^{nat}Cu(^{12}C,X)^{38}Cl$, and $^{nat}Cu(^{20}Ne,X)^{46}Sc$ reactions are shown in Figs. 4(a)–4(f), respectively. The full symbols are from this work, and open symbols are as cited from other experimental data. It is evident from Figs. 4(a)–4(c) that our data for proton reactions agree well with the data of Michel *et al.* [1,2], Schiekel *et al.* [3], and Mills, Steyn, and Nortier

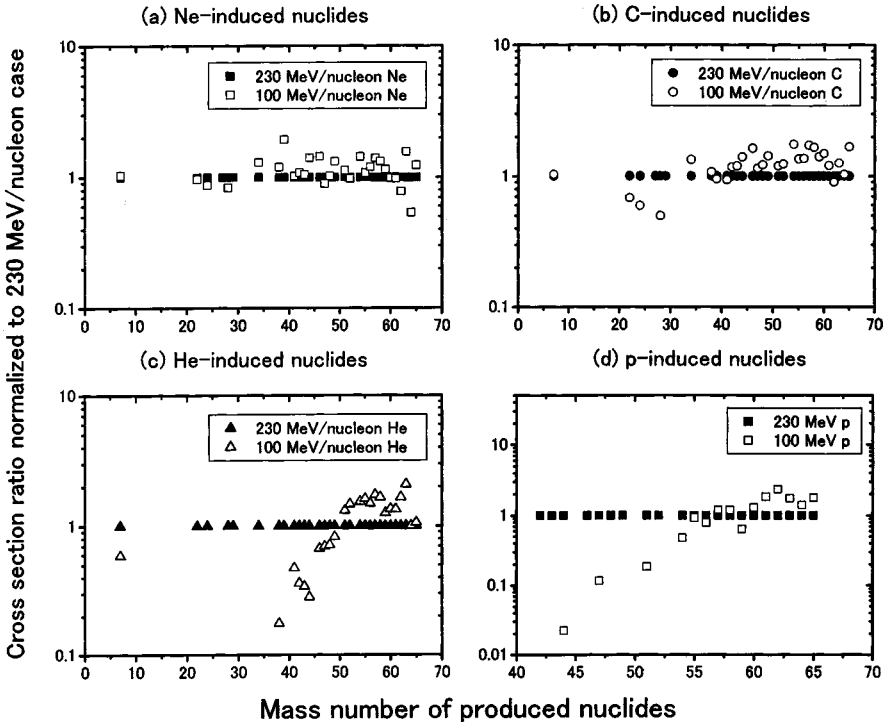

FIG. 6. Energy dependence of nuclides produced in Cu.

TABLE IV. Fitting parameters in Eqs. (6) and (7). "Ne [230]" signifies 230 MeV/nucleon Ne irradiation.

	Ne[230]		C[230]		He[230]		p[230]	
	Value	Error	Value	Error	Value	Error	Value	Error
α_1	7.13	2.28	7.96	2.46	12	3.4	−19.7	35
α_2	−0.596	0.172	−0.603	0.189	−1.05	0.25	0.436	2.01
α_3	1.74×10^{-2}	4.1×10^{-3}	1.75×10^{-2}	4.6×10^{-3}	2.92×10^{-2}	5.8×10^{-3}	5.55×10^{-3}	3.83×10^{-2}
α_4	-1.40×10^{-4}	3.2×10^{-5}	-1.44×10^{-4}	3.5×10^{-5}	-2.35×10^{-4}	4.4×10^{-5}	-1.05×10^{-4}	2.40×10^{-4}
α_5	1.57	0.55	1.95	0.72	1.23	0.4	−23.8	4.7
α_6	−0.109	0.027	−0.166	0.035	−0.136	0.019	0.763	0.179
α_7	1.01×10^{-3}	3.1×10^{-4}	1.91×10^{-3}	4.0×10^{-4}	1.60×10^{-3}	2.2×10^{-4}	-6.52×10^{-3}	1.68×10^{-3}
α_8	2		2		2		2	
α_9	0.481	0.003	0.48	0.002	0.483	0.0013	0.488	0.002
α_{10}	-3.10×10^{-4}	6.0×10^{-5}	-3.05×10^{-4}	3.9×10^{-5}	3.35×10^{-4}	2.4×10^{-5}	-4.17×10^{-4}	3.8×10^{-5}

	Ne[100]		C[100]		He[100]	
	Value	Error	Value	Error	Value	Error
α_1	16.4	4.5	14	4.8	139.7	41.3
α_2	−1.3	0.34	−1.19	0.37	−9.039	2.45
α_3	3.46×10^{-2}	8.1×10^{-3}	3.32×10^{-2}	8.7×10^{-3}	1.92×10^{-1}	4.8×10^{-2}
α_4	-2.75×10^{-4}	6.1×10^{-5}	-2.70×10^{-4}	6.6×10^{-5}	-1.32×10^{-3}	3.1×10^{-4}
α_5	2.12	0.62	2.36	0.6	−1.53	3.56
α_6	−0.153	0.029	−0.165	0.028	−0.0376	0.1388
α_7	1.65×10^{-3}	3.10×10^{-4}	1.78×10^{-3}	3.1×10^{-4}	7.25×10^{-4}	1.33×10^{-3}
α_8	2		2		2	
α_9	0.482	0.0011	0.482	0.001	0.482	0.003
α_{10}	-3.20×10^{-4}	2.1×10^{-5}	-3.27×10^{-4}	2.7×10^{-5}	-3.11×10^{-4}	5.0×10^{-5}

[17]. Figure 4(d) shows that our data also agree well with the data of Michel *et al.* [1,2], Schiekel *et al.* [3], and Mills, Steyn, and Nortier [17] for 100 MeV irradiation but our cross sections are slightly larger than the data of Mills, Steyn, and Nortier [17] for 230 MeV irradiation. As seen in Fig. 4(e), our data for ^{12}C reactions are ~60% larger than the data of Kim *et al.* [4] and in Fig. 4(f), our data for ^{20}Ne reactions are ~60% lower than the data of Hicks *et al.* [5] Generally speaking, our data show good agreement with other data for proton irradiation, but for heavy-ion irradiation our data differ by ~60% from other data. However, considering the large errors and scarcity of existing data, this discrepancy might not be significant. Our data are the first systematic experimental results for heavy-ion irradiation and excitation functions of ^{22}Na, ^{24}Na, and ^{38}Cl production from He, C, and Ne projectiles are given in Fig. 3 as representative examples.

D. Mass-yield distribution of nuclides produced in Cu

The mass-yield distribution of nuclides produced in the Cu pieces is deduced from the reaction cross sections and mass-yield (isobaric yield) distributions of nuclides produced in the Cu piece on the surface irradiated by 230 and 100 MeV/nucleon Ne, C, He, and p ions are shown in Fig. 5.

It is evident from Fig. 5 that the cross section of isobaric yields initially decreases with increasing mass number difference between Cu and the produced nuclide. However, the production cross section then increases for light nuclides, since light nuclides such as ^{7}Be are mainly produced by projectile fragmentation, and do not depend strongly on the target mass number (here Cu, $A\sim64$ amu).

E. Energy dependence of nuclides produced in Cu

The energy dependence of Ne-, C-, He-, and p-induced nuclides on the surface of the Cu target are shown in Figs. 6(a)–6(d), respectively. The vertical axis is the ratio of cross sections obtained by 100 MeV/nucleon projectile energy normalized to 230 MeV/nucleon data. For Ne and C ions in Figs. 6(a) and 6(b), the ratio is almost equal to 1, which means that both cross sections are almost equal and do not depend strongly on the projectile energy. In contrast, for He ions shown in Fig. 6(c), a clear trend is observed, the yields decrease strongly with increasing mass number difference between Cu and the produced nuclide for lower projectile energy of 100 MeV/nucleon and the same trend is seen for protons in Fig. 6(d), where the energy dependence of the mass-yield distribution is even stronger than for He ions.

The strong energy dependence of the mass-yield distribution for light projectile ions reflects the fact that the total energy transferred to the target by the projectile still increases with energy per nucleon, and cross sections increase as can be seen in Figs. 4(a) and 4(b). However, Figs. 4(e) and 4(f) show that production yields level off beyond 100 MeV/

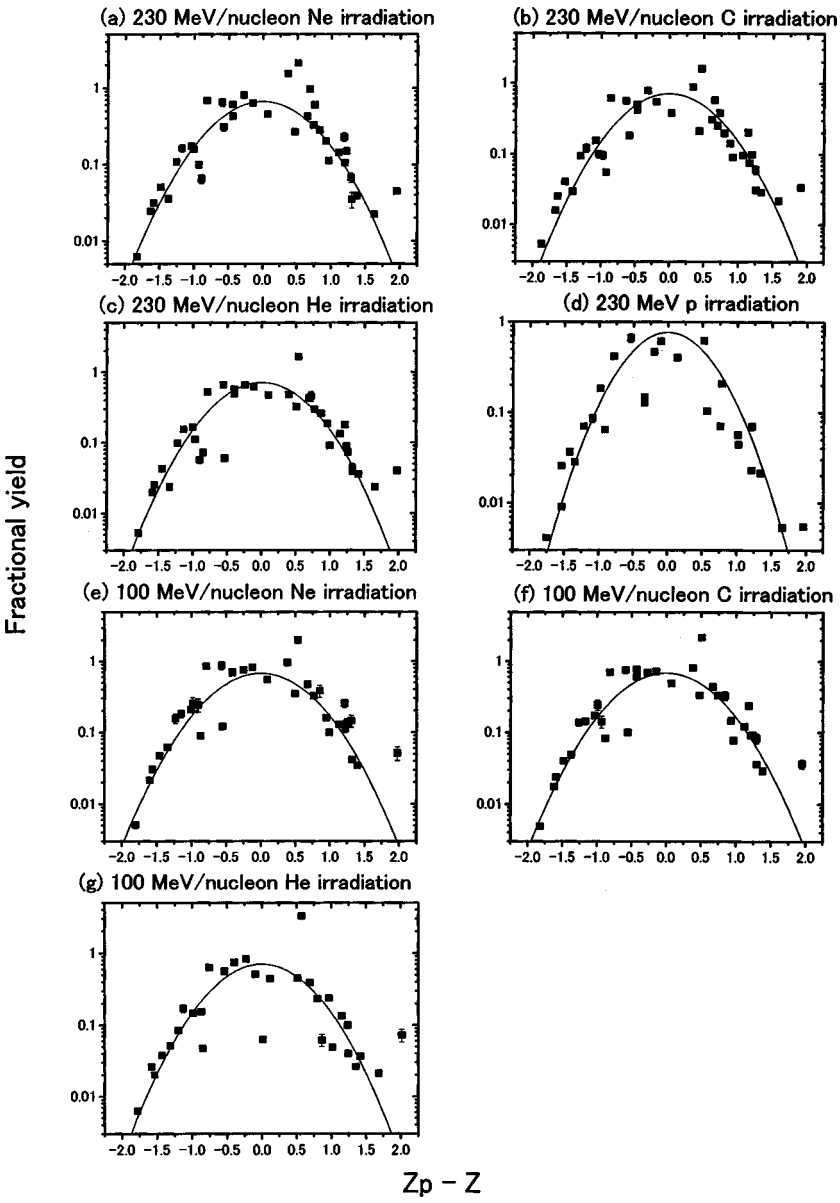

FIG. 8. Normalized charge distribution of nuclides produced in Cu. Points are from data. The curve is from the calculated charge distribution ($A=51$).

nucleon for heavy-ion-induced reactions. Therefore only a weak energy dependence is observed.

F. Projectile mass dependence of nuclides produced in Cu

The projectile mass dependence of nuclides produced in the surface of the Cu target bombarded by 230 and 100 MeV/nucleon Ne, C, He, and *p* ions is shown in Fig. 7. The vertical axis is the ratio of cross sections produced by C, He, and *p* ions normalized to Ne ions. Note that the yield of light spallation products increases with projectile mass and energy as one might expect (see discussion in the preceding section).

V. APPLICATION OF SEMIEMPIRICAL FORMULA TO OBTAIN THE HEAVY-ION-INDUCED SPALLATION CROSS SECTION

For 230 MeV/nucleon Ne, C, He, and *p* and for 100 MeV/nucleon Ne, C, and He ions, we have used a modified form of Rudstam's semiempirical formula [10] by Porile, Cole, and Rudy [6], which assumes an exponential mass-yield distribution and a Gaussian charge distribution to evaluate the cross section of unmeasured nuclides which are stable or have short (or very long) half-lives.

The modified form that has ten parameters to be fitted to the measured cross sections is

$$\sigma(Z,A)=\exp[\alpha_1+\alpha_2 A+\alpha_3 A^2+\alpha_4 A^3 + (\alpha_5+\alpha_6 A+\alpha_7 A^2)|Z_p-Z|^{\alpha_8}], \quad (6)$$

where

$$Z_p=\alpha_9 A+\alpha_{10} A^2. \quad (7)$$

The parameters α_1 to α_4 determine the shape of the mass-yield distribution which is expressed as an exponential function with a third-order polynomial of A. The parameters α_5 to α_7 determine the width of charge distribution. The inclu-

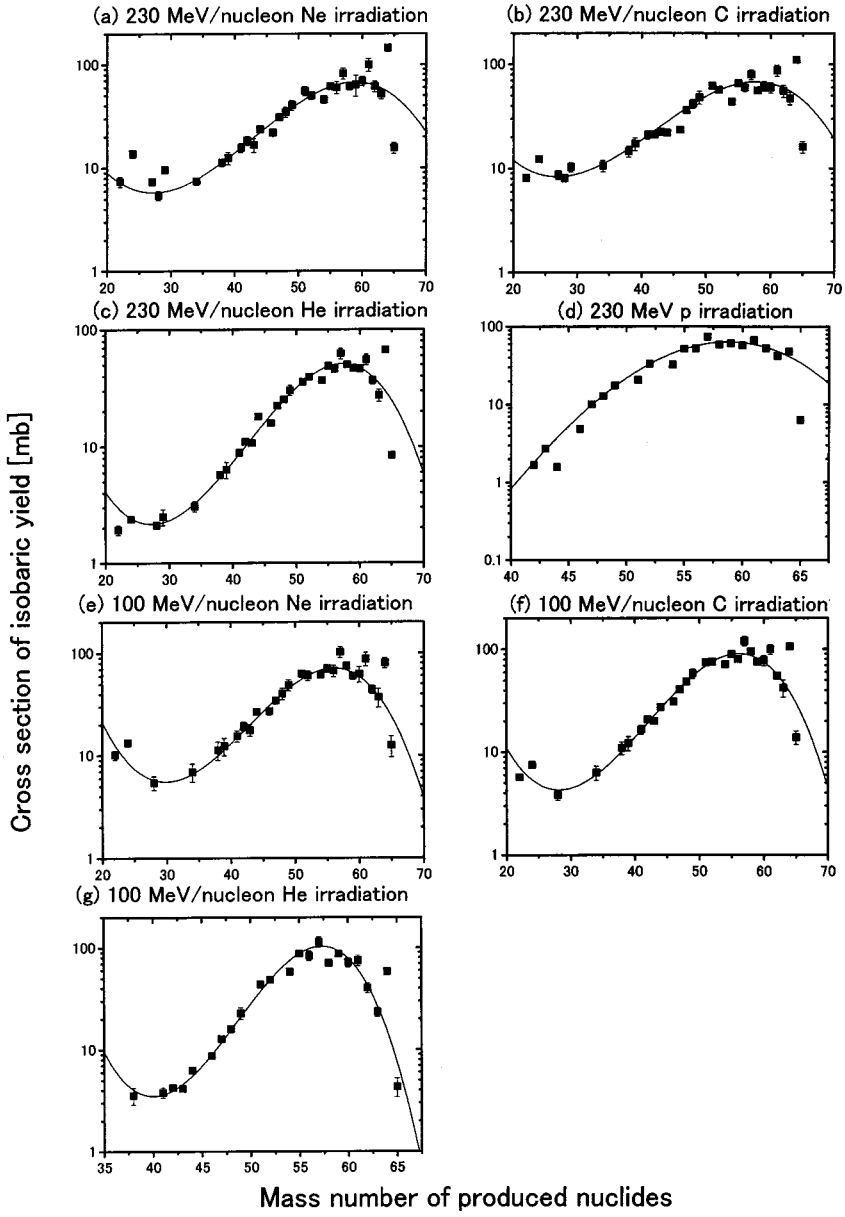

FIG. 9. Comparison of the fitted mass-yield curves with the measurements. Points are from data corrected for unmeasured yields. The curve is from the calculated mass-yield distribution.

sion of two A-dependent terms $\alpha_6 A$ and $\alpha_7 A^2$ allows for a possible mass dependence in the width and the parameter α_8 determines the shape of the charge distribution at a given mass number. In this study, we used $\alpha_8 = 2$ corresponding to a Gaussian distribution. The charge distribution is assumed to be symmetric about the most probable charge Z_p, whose dependence on mass is parametrized by α_9 and α_{10}.

The measured cross sections were fitted with Eqs. (6) and (7) by means of an iterative nonlinear least-square-fit code. In the first iteration, cumulative and independent yields from ^{7}Be to ^{65}Zn (see Table III) were fitted without correction. Then the cumulative cross sections were corrected for isobaric feed-in by means of the calculated progenitor cross sections, and the resulting independent yields were refitted with Eqs. (6) and (7). This procedure usually converges after three to four iterations. The values of the parameters thus obtained are listed in Table IV. The fitted charge distribution and the experimental data are shown in Figs. 8(a)–8(g). In order to compare the independent yields derived from the measured cross sections with the charge distribution, it is convenient to divide both corrected experimental and calculated cross sections by the calculated total isobar cross section in order to obtain fractional isobar yields, f. For the purpose of better display and comparison with previous results, the experimental values f are scaled to an arbitrary common mass number $A = 51$ using the ratio of calculated f values at $A = 51$ and at the actual mass number as a scaling factor. The results are shown in Figs. 8(a)–8(g) for each projectile type and energy, and it is evident that the calculated curves give a good fit to the measured data. Some experimental data scatter from the calculated curves. Especially for 230 MeV proton and 100 MeV/nucleon He irradiation, the experimental data of spallation products which are closer to most probable charge deviate from the calculated curves. From these comparisons in Fig. 8, we estimate that the uncertainties in the fitting procedure are 50% for 230 MeV

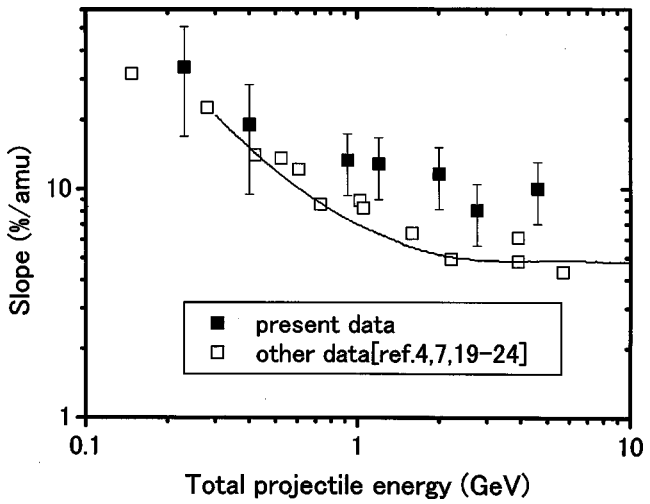

FIG. 10. Slope of the Cu spallation mass-yield curve. The curve is taken from Ref. [9].

proton and 100 MeV/nucleon He irradiation and 30% for others.

The cross sections of unmeasured nuclides were evaluated using Eqs. (6) and (7). These cross sections were added to the experimental yields at the same mass number in order to obtain the total mass-yield distribution. Comparison of the fitted mass-yield curves with the experimental mass-yield distributions are shown in Figs. 9(a)–9(g) and good agreement is obtained.

Cumming *et al.* [9] have examined the energy dependence of the slope in the exponential mass region between $A=38$ and 57 (seen in Fig. 9) for a variety of projectiles interacting with copper. Figure 10 shows the slope of the mass-yield distribution obtained from the present data in this mass region compared to the slopes obtained by other authors [4,7,18–23]. The errors of the present data in Fig. 10 include fit uncertainities as described above. Our data are larger than other data when the total projectile energy is larger than 1 GeV, but the slope is almost constant in this energy region and indicates limiting fragmentation as in other data.

VI. CONCLUSION

We performed irradiation experiments with 230 and 100 MeV/nucleon Ne, C, He, and *p* ions, and obtained the spatial distribution of residual activities of nuclides produced in inserted Cu pieces as a function of the Cu target depth and the mass-yield distributions of nuclides produced on the surface of Cu target.

Our results, in general, agree with other experimental data, and it was found that the projectile dependence of the reaction cross section increases with increasing mass number difference between Cu and the produced nuclide. We also deduced the energy dependence of the reaction yields.

We have used a semiempirical formula to evaluate the cross sections of unmeasured nuclides. These cross sections were added to the experimental yields at the same mass number in order to obtain the experimental mass-yield distribution. We then deduced the slope of the mass-yield distribution. Our data are larger than other data when the total projectile energy is larger than 1 GeV, but the slope is almost constant in this energy region and indicates limiting fragmentation as in other data.

This systematic study should be useful for designing new high-energy heavy-ion accelerator facilities and for benchmark test of the nuclear reaction simulation codes.

ACKNOWLEDGMENTS

We gratefully acknowledge the support and assistance of the accelerator operation staff at HIMAC. We wish to thank the members of the Nakamura Laboratory at the Department of Quantum Science and Energy Engineering, Tohoku University. This work was supported in part by the research project with heavy ions at NIRS-HIMAC.

[1] R. Michel *et al.*, Nucl. Instrum. Methods Phys. Res. B **103**, 183 (1995).
[2] R. Michel *et al.*, Nucl. Instrum. Methods Phys. Res. B **129**, 153 (1997).
[3] Th. Schiekel *et al.*, Nucl. Instrum. Methods Phys. Res. B **114**, 91 (1996).
[4] Y. K. Kim, J. C. Kim, Chang-Bum Moon, S. Y. Cho, Y. H. Chung, and Y. Ohkubo, Nucl. Phys. **A578**, 621 (1994).
[5] K. H. Hicks, T. E. Ward, H. Bowman, J. G. Ingersoll, J. O. Rasmussen, J. P. Sullivan, M. Koike, and J. Peter, Phys. Rev. C **26**, 2016 (1993).
[6] N. T. Porile, G. D. Cole, and C. R. Rudy, Phys. Rev. C **19**, 2288 (1979).
[7] J. B. Cumming, P. E. Haustein, and R. W. Stoenner, Phys. Rev. C **10**, 739 (1974).
[8] J. B. Cumming and R. W. Stoenner, Phys. Rev. C **14**, 1554 (1976).
[9] J. B. Cumming, P. E. Haustein, T. J. Ruth, and G. J. Virtes, Phys. Rev. C **17**, 1632 (1978).
[10] G. Rudstam, Z. Naturforsch. A **21A**, 1027 (1966).
[11] T. W. Armstrong and K. C. Chandler, Report No. ORNL-4869, 1973.
[12] Th. Schwab, GSI Report No. 91-10, 1991; C. Scheidenberger, Ph.D. thesis, Justus-Liebig University, 1994.
[13] H. Hirayama, W. R. Nelson, and D. W. O. Rogers, Stanford University Report No. SLAC-265, 1985.
[14] A. Torii, Y. Uwamino, and T. Nakamura, University of Tokyo Report No. NS-T-468, 1987.
[15] E. Q. Shen, Nucl. Phys. **A491**, 130 (1994).
[16] *Table of Isotopes*, 8th ed., edited by R. B. Firestone and V. S. Shirley (Wiley, New York, 1996).
[17] S. J. Mills, G. F. Steyn, and F. M. Nortier, Appl. Radiat. Isot. **43**, 1019 (1992).
[18] T. Lund, D. Molzahn, B. Bergersen, E. Hagebo, I. R.

Haldorsen, and C. Richard-Serre, Z. Phys. A **306**, 43 (1982).
[19] S. Y. Cho, N. T. Porile, and D. J. Morrissey, Phys. Rev. C **39**, 2227 (1989).
[20] J. P. Whitfield and N. T. Porile, Phys. Rev. C **47**, 1636 (1993).
[21] G. Friedlander, J. M. Miller, R. Wolfgang, J. Hudis, and E. Baker, Phys. Rev. **94**, 727 (1954).
[22] D. W. Barr, Lawrence Berkeley Report No. UCRL-3793, 1957.
[23] P. J. Karol, Phys. Rev. C **10**, 150 (1974).